Path Planning for Laser Cutting Based on Thermal Field Ant Colony Algorithm

Junjie GE, Guangfa ZHANG, Tian CHEN
College of Mechanical Engineering, Shanghai Dianji University, Shanghai 201306, China

***Abstract*—In laser cutting technology, path planning is the key to optimizing cutting quality. Traditional ant colony optimization path planning does not prevent excessive heat effects after processing. This paper addresses the problem of heat accumulation during drilling by introducing a heat factor and a heat threshold into the traditional ant colony algorithm. The heat factor and threshold are used to dynamically control heating and cooling in the path planning process, and the heat factor is updated to update the local pheromone. Then, the improved 2-opt algorithm with the introduced heat factor is combined to parallelly optimize the path, and a thermal field ant colony algorithm is proposed. The simulation experiments and actual cutting results show that the proposed algorithm is more efficient and effective than traditional ant colony algorithm and improved ant colony algorithm in terms of reducing heat accumulation while ensuring fewer empty path, and improving laser cutting processing efficiency and quality.**

***Keywords*—Laser cutting; path planning; ant colony algorithm; thermal field control method**

I. Introduction

Laser cutting technology, known for its high precision and efficiency, is widely used in the manufacturing industry. Path planning plays a crucial role in achieving optimal cutting performance. Traditional path planning methods often fail to reach the optimal solution when dealing with complex conditions, which has led to increasing attention on intelligent optimization algorithms in recent years. Luodengcheng et al. [1] proposed a method that incorporates a potential field factor into the ant colony algorithm to reduce heat accumulation and non-cutting travel distances, thereby ensuring cutting quality. Chang Cuizhi et al. [2] introduced an annealing algorithm to optimize the cutting path of the generalized traveling salesman problem, effectively preventing tool retractions. Makbul Hajad et al. [3] treated all pixels in an image as potential perforation positions and proposed a simulated annealing algorithm combined with adaptive large neighborhood search, which reduced both computational time and path length. Bonfim Amaro Junior et al. [4] improved the heuristic search in the inheritance algorithm, yielding better solution quality and shorter computation time in laser cutting path planning. Song Lei et al. [5] designed a dual-chromosome encoding mechanism to jointly solve the cutting starting point and path planning problem, reducing both non-cutting travel distances and processing temperature. Wu Yanming et al. [6] employed a greedy algorithm for plate processing path planning, optimizing parameter grouping to achieve the optimal path while ensuring high-quality processing. Zhou Rui et al. [7] improved the genetic algorithm to avoid non-cutting travel and cutting conflicts, enhancing the algorithm's convergence.

The intelligent algorithms used in path planning above aim to minimize non-cutting travel and avoid heat accumulation [8]. However, while preventing heat accumulation, they do not necessarily minimize non-cutting travel and computational time. Through the detection of heat accumulation during actual laser cutting, it has been observed that the temperature is highest at the perforation starting point of the cutting element. To address the phenomenon of "laser punching" caused by excessive temperature at the perforation, this paper proposes a thermal field ant colony algorithm. This algorithm incorporates a heat matrix when initializing ant colony parameters, optimizing the probability of visiting cities and updating local pheromones. At the same time, a heat factor-based heuristic algorithm is introduced to parallelly optimize the cutting path.

II. Laser Cutting Path Planning and Design

The laser cutting process flow [9] is shown in Fig. 1. When cutting thicker materials such as carbon steel and stainless steel, achieving high precision and quality requires the incorporation of perforation techniques into the cutting parameter setup [10]. Perforation techniques mainly include pulsed perforation and explosive perforation. In pulsed perforation, a high peak power pulsed laser beam strikes the material surface, rapidly melting or vaporizing the material in a localized area to form a small hole. Explosive perforation, on the other hand, uses a lower-power continuous laser beam to act on the material surface, continuously heating it until the material melts and forms a hole. However, improperly set perforation parameters can lead to heat accumulation on the material surface [11], causing thermal expansion and deformation of the material. This results in a decrease in cutting precision and may even damage components such as optical lenses and focusing lenses, thereby increasing equipment maintenance costs. Therefore, path planning before setting cutting parameters is particularly important.

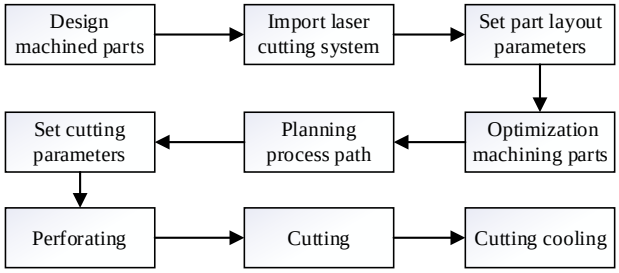

Fig. 1. Laser cutting process.

A. Laser Cutting Path Modeling

First, the feature points of each graphic element are obtained as the starting coordinates for the path planning of each element. For closed polygonal elements, the element contour is decomposed into arcs and straight lines, and the connection points between these lines and arcs are taken as the feature points of the element. For closed circles and ellipses, their feature points are defined by dividing the shape into four equal parts. The start and end points of an arc are calculated as shown in Eq. (1).

$$\begin{cases} x_s = x_c + R \cdot \cos(\theta_s) \\ y_s = y_c + R \cdot \sin(\theta_s) \\ x_e = x_c + R \cdot \cos(\theta_e) \\ y_e = y_c + R \cdot \sin(\theta_e) \end{cases} \tag{1}$$

In the above formula, $\{x_c, y_c\}$ represents the coordinates of the arc center, RRR is the radius of the arc, and (θ_s, θ_e) denote the start and end angles of the arc. $\{x_s, y_s\}$ and $\{x_e, y_e\}$ represent the coordinates of the arc's starting and ending points, respectively.

Using this formula, the feature points of the part contours are determined, as shown in Fig. 2. The closed elements are defined as {Part 1, Part 2, Part 3}, with each closed element corresponding to city coordinate points as follows: {v11, v12, v13, v14, v15, v16, v17, v18, v19}for Part 1, {v21, v22, v23 }for Part 2, and {v31, v32, v33, v34 } for Part 3.

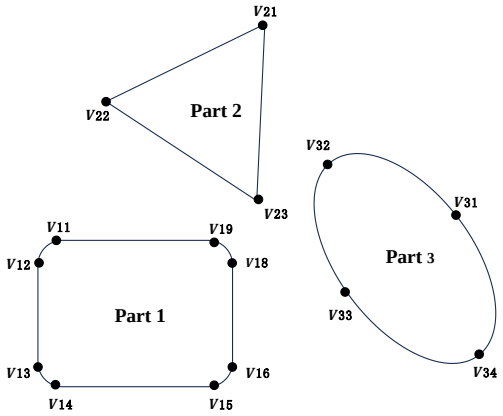

Fig. 2. Method of obtaining feature points of part contour.

Let the total path length L be defined as the total distance traveled by the laser, including all cutting path segments and non-cutting movement path segments from the starting point. The total cutting length is expressed in Eq. (2):

$$L = \sum_{i=1}^{n} d_i + \sum_{j=1}^{m} m_j \tag{2}$$

In this equation, d_i represents the length of the cutting path required for the i-th part, n is the total number of parts in the cutting path, m_j represents the length of the non-cutting movement path to the j-th part, and m is the total number of non-cutting paths in the cutting sequence.

B. Thermal Field Modeling

During the cutting process, if the perforation time is set too long or the perforation power too high, the starting area of the cut part can become overheated, causing a "punching" phenomenon. Therefore, thermal factors in laser cutting also need to be considered in path planning. The temperature rise ΔT at a point on the material at time t can generally be estimated using the heat conduction formula [12]. Assuming an initial temperature T of the material, the temperature rise at a certain point under the effect of the laser heat source is given by Eq. (3):

$$\Delta T = \frac{P \cdot \exp\left(-\frac{r^2}{4 \cdot a \cdot t}\right)}{\rho \cdot c \cdot \sqrt{4 \cdot \pi \cdot a \cdot t}} \tag{3}$$

In this equation, P is the laser power, ρ is the material density, c is the specific heat capacity of the material, α is the thermal diffusivity, and r is the distance from the point to the laser heat source.

During laser cutting, heat is mainly dissipated through convective heat transfer to the surrounding air and through thermal conduction within the material itself [13]. Based on the above formula for temperature rise, the cooling temperature drop can be expressed as Eq. (4):

$$\Delta T = \exp\left(-\frac{h \cdot A}{m \cdot c} \cdot t\right)\left(T_S - T_N\right) + \varepsilon \cdot \sigma \cdot A \cdot \left(T_S^4 - T_N^4\right) \tag{4}$$

where h is the convective heat transfer coefficient, A is the surface area, m is the material mass, ε is the emissivity of the material, σ is the Stefan-Boltzmann constant, T_s is the surface temperature of the material, and T_N is the ambient temperature.

Given the parameters for heating with a laser power P =1000 W, a cutting material of steel with density ρ = 7800 kg/m3, specific heat capacity c= 500 J/kg · K, and thermal diffusivity α=1×10−5 m2/s. For cooling, assume the surface temperature Ts=60 ◦ C, ambient temperature T_N = 20 ◦ CT, convective heat transfer coefficient h=25 W/m2 · K, emissivity ε=0.7, Stefan-Boltzmann constant σ= 5.67×10−8 W/m2 · K4, and material mass m=0.1 kg. The resulting function plots for the temperature rise and cooling temperature drop of the material during laser cutting are shown in Fig. 3.

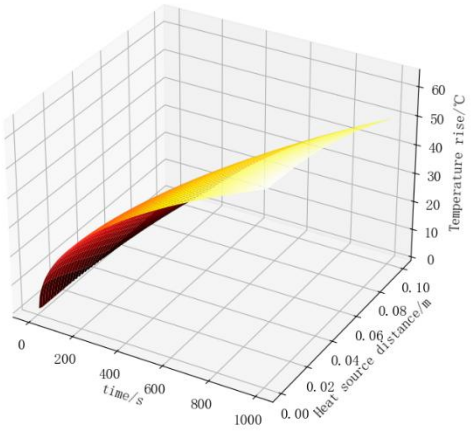

(a) Plate temperature function

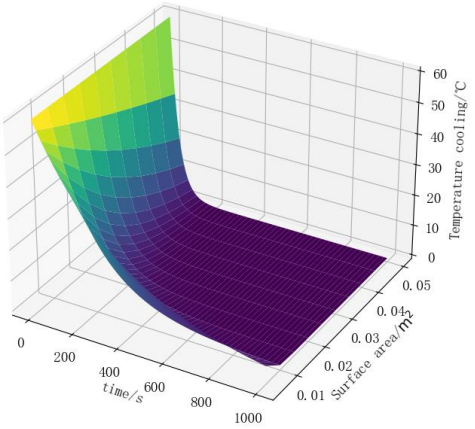

(b) Plate cooling function

Fig. 3. Temperature change of laser cutting sheet.

To effectively control heat accumulation in path planning, it is essential to treat the effect of the laser heat source as a thermal conduction process. Based on the model described in Eq. (3), we can estimate the temperature rise at each point along the cutting path and avoid reheating high-temperature areas during path planning. To achieve this, we define a heat threshold in the thermal-field ant colony algorithm. If the temperature rise ΔT at a given point exceeds this threshold, the path planning algorithm should avoid immediate reprocessing of that point, instead prioritizing areas with lower heat levels for cutting. This approach helps to control heat distribution effectively. In addition to considering the temperature rise caused by laser power, the cooling process's impact on temperature must also be taken into account. This heat threshold can be dynamically adjusted by incorporating the cooling effect as described in Eq. (4), allowing for effective control of overheated areas during the cutting process.

III. Thermal Field Ant Colony Algorithm

A. Description of Thermal Field Ant Colony Algorithm t

Ant Colony Optimization (ACO) [14] is a stochastic optimization algorithm based on simulating the foraging behavior of ants, introduced by Marco Dorigo in the 1990s. This algorithm is particularly suitable for combinatorial optimization problems, such as path optimization. However, ACO tends to get stuck in local optima, has a slower convergence speed, and does not account for heat accumulation in the material during laser cutting. To address these issues, this study incorporates thermal fields and a heat factor into the ACO. Each "city" has a thermal field within a certain range, wherein neighboring points influence each other's temperature. The probability of each ant selecting a city is affected by the heat factor, and a heat threshold is set—when the heat on a path segment exceeds this threshold, the algorithm reduces the probability of selecting this segment, favoring cooler regions to control heat distribution. The heat factor $h(i,j)$ is calculated as shown in Eq. (5):

$$h(i,j)=\begin{cases} e^{-H[i,j]}, -H[i,j] > heat_{\max} \\ 1, others \end{cases} \tag{5}$$

where i is the index of the current city, j is the next city chosen by the ant, $H[i,j]$ represents the thermal matrix between these cities, and $heat\_max$ is the maximum heat threshold between two cities.

The probability of city selection in the heat-field ACO, modified by the heat factor, is shown in Eq. (6):

$$P_{ij}=\frac{(\tau_{ij})^{\alpha}\cdot(\eta_{ij})^{\beta}\cdot h_{ij}}{\sum_{k\in allowed}(\tau_{ij})^{\alpha}\cdot(\eta_{ij})^{\beta}\cdot h_{ik}} \tag{6}$$

where τ_{ij} represents the pheromone concentration between cities i and j, η_{ij} is the heuristic information, and α and β are importance factors for pheromone and heuristic information, respectively. *allowed* is the set of all cities available for selection, and k is the index of selectable cities.

To enhance global search capability and identify optimal paths, a roulette-wheel selection [15] is employed for probabilistic city selection, as mathematically expressed in Eq. (7):

$$P_{ck}=\frac{P_{ij}}{\sum_{i=1}^{n}P_{ij}} \tag{7}$$

where P_{ij} is the probability calculated in Equation (6), $r \in [0,1]$ is a random number, and k is the minimum index for which $P_{ck} \geq r$, making k the selected target city's index.

In the heat-field ACO, after each ant selects the next city, it locally updates the pheromone concentration on that path segment. This local pheromone update balances pheromone accumulation and evaporation to prevent path selection bias caused by a single heat factor. Following each iteration, the global pheromone is updated to speed up convergence to the optimal solution, as shown in Eq. (8):

$$\tau_{ij} = \begin{cases} (1-\rho_m)\cdot\tau_{ij} + \rho_m \cdot \tau_i, \\ \tau_{ij} \in local \\ (1-\rho_g)\cdot\tau_{ij} + \rho_g \cdot \Delta\tau_{ij}, \\ \tau_{ij} \in global \end{cases} \quad (8)$$

where ρ_{m} is the local pheromone evaporation factor, τ_{i} is the initial pheromone concentration to prevent pheromone levels from dropping too low, ρ_{g} is the global pheromone evaporation factor, and $\Delta\tau_{ij}$ is the additional pheromone added along the optimal path.

As ants pass each city, a heating and cooling mechanism is applied to the thermal matrix to reflect accumulated heat from laser cutting, preventing multiple selections of high-heat paths. Meanwhile, during city searches, already visited cities and their surrounding areas cool down, controlling excessive heat accumulation and improving path selection quality. The heating and cooling mechanisms for the thermal matrix are shown in Eq. (9) and Eq. (10):

$$\Delta H_{ij} = P \cdot \exp(-\frac{d_{ij}^2}{\gamma \cdot t}) \quad (9)$$

$$H[i,j] = \begin{cases} H[i,j]\cdot(1-C)\cdot t, \\ H[i,j] \geq heat_{\min} \\ heat_{\min}, \\ others \end{cases} \quad (10)$$

where ΔH_{ij} is the thermal matrix increment, P is the heat coefficient, d_{ij} is the distance between cities i and j, t is the step count, γ is the diffusion coefficient controlling heat dissipation speed, C is the cooling coefficient, and $heat\_min$ is the minimum heat threshold.

To avoid local optima, this study introduces an improved 2-opt [16] algorithm after each ant completes its path based on pheromone selection. Fig. 4 illustrates the 2-opt algorithm optimized path search process.

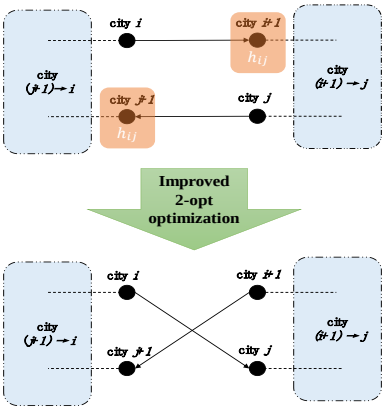

Fig. 4. Improved 2-opt algorithm to optimize the path method.

The core idea is to select two sub-paths on a given route and reverse one portion to check if a shorter total path length can be achieved. Whether to accept the new path is determined by the thermal matrix in Eq. (5), with the acceptance probability shown in Eq. (11):

$$P_{ij} = \exp(-\frac{L_{i,i+1} - L_{i,i}}{h_{ij}}) \quad (11)$$

where $L_{i,i+1}$ is the path length between city i and $i+1$, $L_{i,j}$ is the path length between cities i and j, and h_{ij} is the heat factor from Eq. (5).

B. The Implementation Steps of Path Planning of Thermal Field Ant Colony Algorithm

The path planning in the thermal-field ant colony algorithm first extracts the feature points of each part after laser cutting layout, as illustrated in Fig. 4. These feature points are placed into corresponding arrays to avoid redundant selection of the same geometric element later in the process. Then, the Euclidean distance matrix for each pair of feature points is computed, and the pheromone matrix is initialized. Since solution construction among ants is independent, the optimal path for each ant is calculated in parallel during a single iteration, which reduces computation time. The process terminates upon reaching the maximum number of iterations, after which the part numbers are sorted by shortest path order and output. The detailed procedure is depicted in Fig. 5.

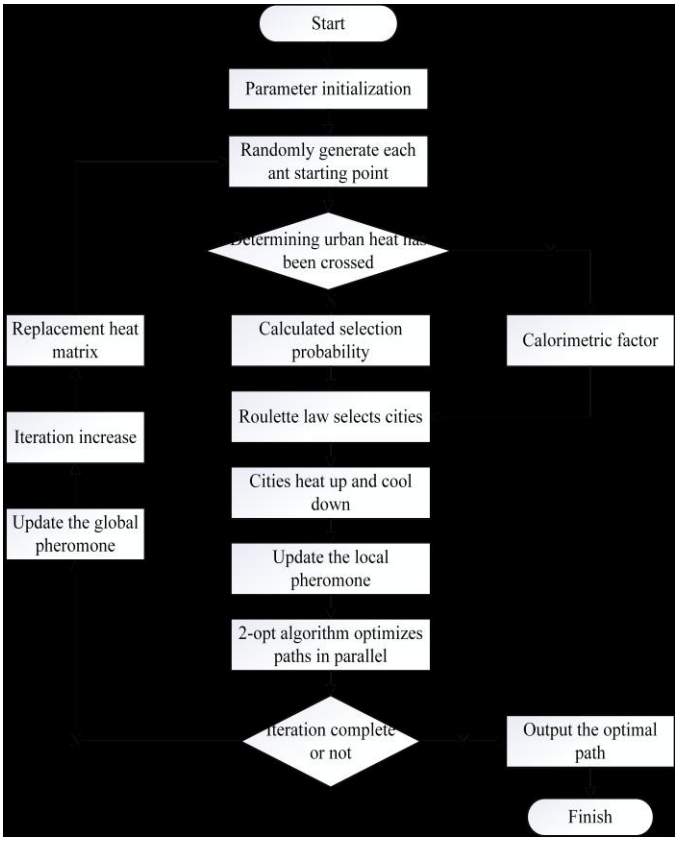

Fig. 5. Algorithm flow chart.

IV. Experiment and Result Analysis

A. Path Planning Experiment

According to the path planning algorithm in this paper, the experimental objects are the parts after nesting, placed on the cutting plate. The feature points are extracted from the DXF file using geometric information as city coordinates. The operating system used in this experiment is Windows 11, with an Intel i5-12400F CPU, and the development environment is PyCharm. Based on the study [17] and multiple tests, the parameters of the algorithm were adjusted to their optimal values: the number of ants $m = 50$, pheromone factor $\alpha = 1$, heuristic function factor $\beta = 5$, global evaporation factor $\rho_g = 0.1$, local evaporation factor $\rho_m = 0.05$, and the maximum number of iterations $iter_{max} = 100$. The thermal field parameters are listed in Table I. The initial thermal matrix H in the table has n rows and n columns, where n represents the number of cities, the number of feature points in the DXF layout.

TABLE I. Thermal Field Parameters

Parameters	Value
Initial heat matrix H	$\begin{bmatrix} 0 & 1.0 & \dots & 1.0 \\ 1.0 & \ddots & \dots & \vdots \\ \vdots & \dots & \ddots & 1.0 \\ 1.0 & \dots & 1.0 & 0 \end{bmatrix}$
Heat threshold $heat_{max}$	0.5
Heating factor P	0.2
Cooling factor C Heat loss γ	0.95 0.05

The result of the experiment is to calculate the time, the path length and the heat matrix when cutting the plate. The optimal path ant heat value of Thermal Field ACO(TF-ACO) is shown in Fig. 6. Compared with Traditional ACO(T-ACO) and Improved ACO(I-ACO), the convergence curve of the improved ant colony algorithm based on study [18] and the convergence curve of the shortest path and the average path of ants is shown in Fig. 6:

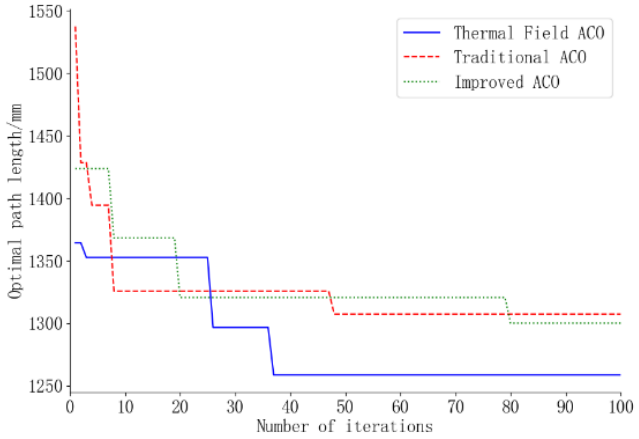

(a) Shortest path convergence curve comparison.

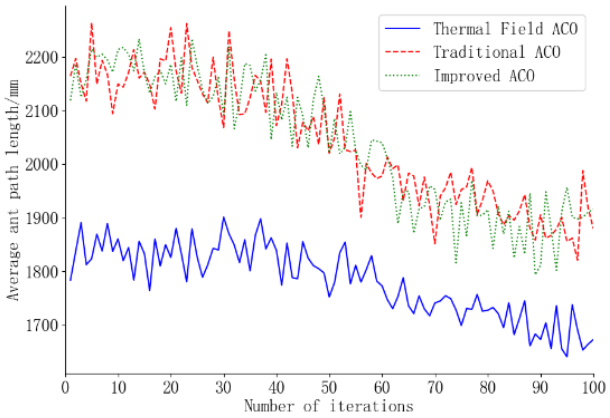

(b) Comparison of ant average path convergence curves.

Fig. 6. Comparison of convergence curves.

When compared to the traditional ant colony algorithm and the improved ant colony algorithm, the convergence curves of the shortest path and the average path length of the ants for the improved algorithm are also depicted in Fig. 6, based on study [18]. After multiple tests, the fastest convergence times, shortest path lengths, and average path lengths of the ants for the three algorithms are shown in Table II.

TABLE II. Optimal Solutions of each Algorithm

Algorithm type	Maximum convergence times/times	Minimum path length /mm	Average ant path length /mm
T-ACO	80	1307.34	1915.97
I-ACO	49	1300.15	1879.26
TF-ACO	38	1250.66	1672.95

From the figures and tables above, it can be observed that compared to the traditional and improved ant colony algorithms, the thermal-field ant colony algorithm reduces the fastest convergence time by approximately 52.5% and 22.4%, respectively. The shortest path length is improved by approximately 4.5% and 3.8%, and the optimal average path length is improved by approximately 14.5% and 12.3%. This demonstrates that the improved code in this paper not only prevents heat accumulation but also improves the optimal path.

In this simulation experiment, the optimal solutions obtained from the three algorithms were plotted on the DXF part base map after nesting, as shown in Fig. 7. Panel (a) displays the base map with numbered parts, showing 15 distinct geometric elements. After computing the geometric features, a total of 71 feature points are derived as the city coordinates for the path planning algorithms. Based on the feature point sequence in the base map, the path planning cutting order for each algorithm is as follows: Traditional ACO: 46, 51, 55, 49, 62, 68, 3, 7, 10, 14, 22, 18, 33, 37, 43. Improved ACO: 22, 17, 18, 41, 36, 37, 45, 49, 50, 55, 68, 63, 3, 8, 13. Thermal-field ACO: 4, 67, 58, 49, 55, 54, 46, 42, 37, 36, 18, 30, 17, 13, 6.

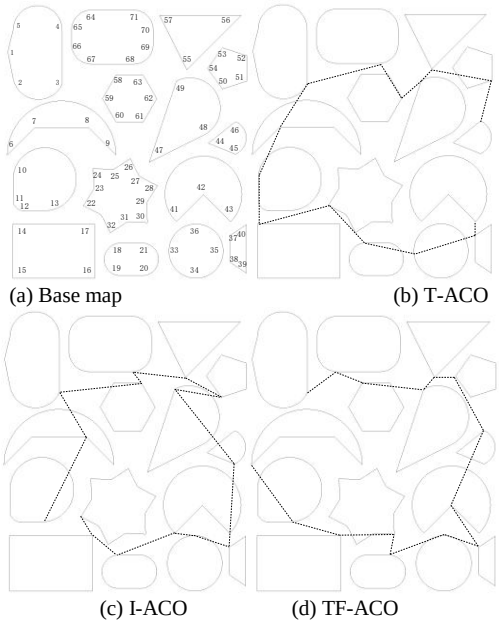

(a) Base map (b) T-ACO

(c) I-ACO (d) TF-ACO

Fig. 7. Feature point diagram and path comparison diagram.

The optimal path heat matrix is also shown in Fig. 8. From this figure, it can be observed that by introducing the heating and cooling factors, most of the city heat values did not exceed the initially set thermal threshold. While the ants selected the optimal path, they also effectively controlled the heat accumulation, avoiding the selection of high-heat cities as the cutting start points during perforation. This mechanism ensures that the material does not overheat during cutting, which could otherwise negatively affect the cutting quality.

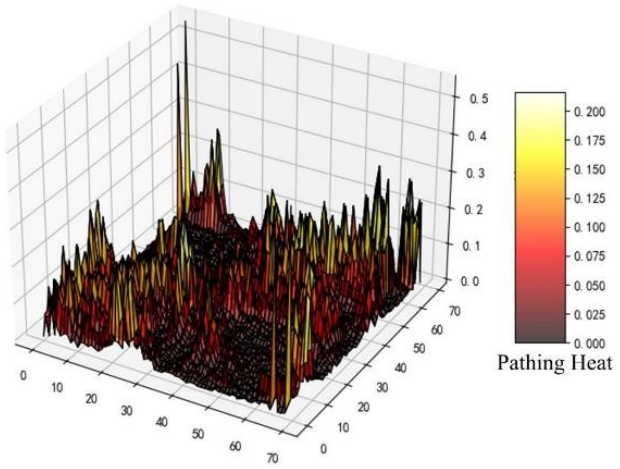

Fig. 8. Heat distribution diagram of optimal path.

B. Cutting Experiment

In this cutting experiment, a flatbed laser cutting machine was used for comparison. The DXF file from Fig. 7 served as the cutting object for the experiment. The laser cutting machine model is FLM3015, equipped with a continuous fiber laser of the model EFRC-3000-E, with a rated output power minimum of 2900W, a maximum of 3100W, and a measured center wavelength of 1080nm. The working voltage is 380VAC, and the output fiber core diameter is 250um. Fig. 9 shows the laser cutting machine used for this experiment.

Fig. 9. Experimental laser cutting machine.

Carbon steel with dimensions 500mm × 500mm × 6mm was selected as the cutting material for the experiment. Prior to cutting, a perforation process was applied to compare the effects of different algorithms on the temperature of the material after perforation. The laser cutting process parameters are shown in Table III.

TABLE III. PROCESS PARAMETERS

Parameters	Value	Unit
Cutting speed	100	mm/s
Barometric type	oxygen	
Atmospheric pressure Peak power Punch grade Progressive time	5 1000 first-order 1000	BAR W ms

Based on the process parameters mentioned, the optimal paths obtained from the three path-planning algorithms were imported into the laser cutting system for cutting experiments. During the experiment, an infrared thermometer was used to measure the surface temperature of the material in real-time, recording the maximum temperature reached by each algorithm during the cutting process. The ambient temperature during the experiment was 20°C. The data recorded for planning time, processing time, and average cutting temperature for each algorithm are shown in Table IV.

TABLE IV. CUTTING COMPARISON OF EACH ALGORITHM

Algorithm type	Plan time /s	Cutting time /s	Maximum cutting temperature /℃
T- ACO	4.35	74.49	262.32
I-ACO	3.81	72.13	257.09
TF-ACO	3.70	70.06	209.87

From the table, it can be observed that compared to the traditional and improved ant colony algorithms, the thermal-field ant colony algorithm resulted in approximately 14.9% and 2.8% improvement in planning time, 5.9% and 2.8% improvement in cutting time, and 19.9% and 18.4% improvement in the maximum cutting temperature, respectively. These results indicate that the thermal-field ant

colony algorithm not only effectively avoids heat accumulation but also reduces the temperature increase while maintaining optimal planning and cutting times. This algorithm better controls the heat distribution during the cutting process, minimizing overheating, thus ensuring cutting quality and the integrity of the workpiece while improving path planning and cutting efficiency.

V. CONCLUSIONS

In comparison to the traditional and improved ant colony algorithms, the thermal-field ant colony algorithm presented in this study demonstrates significant advantages in laser cutting path planning. Specifically, the algorithm reduced the number of iterations by 22.4% to 52.5%, the planning computation time by 2.8% to 14.9%, the non-cutting travel path length by 12.3% to 14.5%, the cutting time by 2.8% to 5.9%, and the maximum cutting temperature by 18.4% to 19.9%. These results indicate that the thermal-field ant colony algorithm not only effectively shortens the cutting travel and processing time but also reduces the perforation issues caused by heat accumulation during laser cutting, preventing the occurrence of "burn-through" and lowering the overall cost of the laser cutting process.

However, certain environmental factors such as smoke, dust, and the material surface's emissivity in the experimental setting have introduced some uncertainty in the temperature measurement results. Therefore, future research will focus on further optimizing the path planning algorithm and improving the accuracy of temperature monitoring to better adapt to real-world production environments.

ACKNOWLEDGMENT

Funding: The work described in this article was supported by Shanghai Multi-Direction Die Forging Engineering Technology Research Center (20DZ2253200); Supported by Intelligent Manufacturing Industry College of Shanghai Lingang New Area (B1-0299-21-023). Shanghai Local College Capacity Building Project (22010501000).

Conflicts of Interest: The authors declare that there are no conflicts of interest.

REFERENCES

[1] Luo Dengcheng, Wang Hongjian, Li Yongliang, et al. Potential field-ant colony algorithm planning of laser cutting path [J]. Laser Journal,2023,44(10):14-18.

[2] Chang Cuizhi, Gao Wenliang, Yan Penghui, et al. Annealing algorithm of double-stranded gene for laser cutting path optimization [J]. Journal of Wuhan Polytechnic University,2023,45(03):331-336.

[3] Hajad M ,Tangwarodomnukun V ,Jaturanonda C , et al.Laser cutting path optimization using simulated annealing with an adaptive large neighborhood search[J].The International Journal of Advanced Manufacturing Technology,2019,103(1-4):781-792.

[4] Junior A B ,Carvalho D N G ,Santos C M , et al.Evolutionary Algorithms for Optimization Sequence of Cut in the Laser Cutting Path Problem[J].Applied Sciences,2023,13(18):

[5] Song Lei, Wang Xinxin, Liu Xiaoyan, et al. Two-chromosome Genetic algorithm optimization of Laser Cutting process Path [J]. Forging & Stamping Technology,2021,46(10):119-125.

[6] Wu Yanming, Cao Ning, Li Feiya, et al. Research on Optimization Algorithm of plate porous Processing Path based on Greedy Algorithm [J]. Journal of Hefei University of Technology (Natural Science Edition),2022,45(06):742-745+759.

[7] Zhou Rui, Ma Hanwu. Path planning of laser cutting collaborative work based on improved Genetic algorithm [J]. Logistics Technology,2021,44(10):50-55.

[8] Zhou Zhichao, Cui Quanfa, Yang Yanlong, et al. Analysis of heat affected zone in laser cutting [J]. Physical Measurement and Testing,2019,37(01):14-17.

[9] Yilbas B ,Arif A .Laser cutting of steel and thermal stress development[J].Optics and Laser Technology, the lancet, 2010 (4) : 830-837.

[10] YAN Shu, Li Lijun, Li Juan, et al. Review on surface quality of laser cutting sheet [J]. Laser Technology,2005,(03):270-274.

[11] Teng Jie, Wang Binxiu. Analysis and Solution of Common Problems in Laser Cutting Process [J]. Electromachining & Mold,2009,(04):60-61. Xu Luning, WANG Xiao, ZHANG Yongkang. Process treatment of laser cutting sheet metal [J]. Applied Laser,2002,(06):533-538.

[12] Xue Zhongming, Gu LAN, Zhang Yanhua. Numerical simulation of Temperature field in laser welding [J]. Chinese Journal of Welding,2003,(02):79-82+0.

[13] Zhou Leping, Tang Dawei, Du Xiaoze, et al. High power laser weapon and its cooling system [J]. Advances in Laser and Optoelectronics,2007,(08):34-38.

[14] Duan Haibin, Wang Daobo, Zhu Jiaqiang, et al. Progress in theory and application of ant colony algorithm [J]. Control and Decision,2004,(12):1321-1326+1340.

[15] Zhu Qing-Bao, Zhang Yulan. Robot path Planning Ant Colony Algorithm based on raster Method [J]. Robot,2005,(02):132-136.

[16] Li Jun, Tong Zhao, Wang Zheng. A parallel ACS-2-opt algorithm for solving TSP problems [J]. Computer Science,2018,45(S2):138-142.

[17] Zhan Shichang, Xu Jie, Wu Jun. Ant colony algorithm in the algorithm of optimal parameter selection [J]. Science, 2003, (5) : 381-386. The DOI: 10.13774 / j.carol carroll nki KJTB. 2003.05.008.

[18] Hou Puliang, Liu Jianqun, Gao Weiqiang. Research on Path Optimization of Laser Cutting based on Improved Ant Colony Algorithm [J]. Mechanical and Electrical Engineering,2019,36(06):653-657.